J Appl Electrochem (2009) 39:1157–1162
DOI 10.1007/s10800-008-9774-1

ORIGINAL PAPER

An amorphous Si thin film anode with high capacity and long cycling life for lithium ion batteries

L. B. Chen · J. Y. Xie · H. C. Yu · T. H. Wang

Received: 25 May 2008 / Accepted: 23 December 2008 / Published online: 8 January 2009

Abstract A Si thin film of thickness 275 nm was deposited on rough Cu foil by magnetron sputtering for use as lithium ion battery anode material. X-ray diffraction (XRD) and TEM analysis revealed that the Si thin film was completely of amorphous structure. The electrochemical performance of the Si thin film was investigated by cyclic voltammetry and constant current charge/discharge test. The film exhibited a high capacity of 3,134 mAh g^{-1} at 0.025 C rate. The capacity retention was 61.3% at 0.5 C rate for 500 cycles. An island structure formed on the Cu foil substrate after cycling adhered to the substrate firmly and provided electrical connection. This is the possible reason for the long cycling life of Si thin film anode. Moreover, the cycling performance was further improved by annealing at 300 °C. The Li^+ diffusion coefficients (D_0) of Si thin film, measured by cyclic voltammetry, are 1.47 × 10^{-9} cm^2 s^{-1} and 2.16 × 10^{-9} cm^2 s^{-1} for different reduced peaks.

Keywords Si thin film · Long cycling life · Magnetron sputtering · Lithium ion battery · Anode

1 Introduction

There is an increasing demand for lithium ion batteries with high energy density and long cycling life, with the rapid development of portable electronics and (hybrid) electrical vehicles. Si is the most promising anode material for high energy lithium ion batteries because it has the highest specific capacity (4,200 mAh g^{-1}) than any other anodes studied to date [1]. However, Si shows a drastic volume expansion/contraction during Li^+ insertion/extraction. This causes the pulverization of Si particles and loose contacts between Si particles and current collector resulting in the mechanical instability and poor cyclability. The volume change and adherence to current collector of Si active material have been regarded as the key factors to the electrochemical stability of Si anodes [2, 3]. Therefore, amorphous Si thin film anodes have been investigated extensively because of their smaller volume change and strong adhesion between the active material and current collector.

Several techniques have been used to fabricate Si thin films for lithium ion battery anodes. Chemical vapor deposition (CVD) was firstly adopted by Bourderau et al. [4]. The Si thin film exhibited a capacity of over 1,000 mAh g^{-1}, but the cycling performance was very poor because the thickness was over 1.2 μm. Jung et al. [5, 6] also fabricated Si thin film anode by CVD. Although they achieved very high capacity, the cyclability of this film was still unsatisfactory because of undesirable parasites and pores that produced mechanical cracking upon cycling. Xia et al. [7] reported amorphous Si thin film anodes prepared by pulsed laser deposition. Takamura and co-workers studied Si thin film anodes fabricated by vacuum deposition [8–11]. They succeeded in prolonging the cycle life of Si thin film by increasing the surface roughness of the current collector. This film showed excellent cyclability and high capacity. Among the various methods for preparing film materials, magnetron sputtering is the most appropriate process to fabricate dense Si thin film

L. B. Chen (✉) · H. C. Yu · T. H. Wang
Micro-Nano Technologies Research Center, Hunan University, Changsha 410082, China
e-mail: libaochen@gmail.com

J. Y. Xie
Energy Science and Technology Laboratory, Shanghai Institute of Microsystem and Information Technology, Chinese Academy of Sciences, Shanghai 200050, China

with strong adhesion to the substrate. Some groups have investigated Si thin film anodes prepared by magnetron sputtering [12–17]. However, the cycle life of the Si thin films fabricated by this technique still requires improvement. This paper reports Si thin film anodes prepared by magnetron sputtering with high capacity and long cycle life. Cycling performance of the film was further improved by annealing at 300 °C. The morphology change after cycling was investigated to verify the excellent cyclability.

2 Experimental

Si thin films were prepared in an ANELVA SPC-350 multi-target magnetron sputtering system. The samples were deposited simultaneously on both Si wafer for thickness measurement and Cu foil with a surface roughness of 0.4 μm (RMS) for electrochemical measurements. The target was N-type monocrystalline Si. The target-substrate distance of the sputtering system was 5 cm. After the base pressure reached 2×10^{-4} Pa, Ar (99.999%) was introduced into the chamber. The working pressure was kept at 0.32 Pa. Si thin films were deposited using a constant radio frequency (rf) power supply of 60 W. The film thickness was controlled by deposition time. The amount of deposited Si was calculated assuming a density of 2.33 g cm^{-3} for the Si thin film.

The morphology and accurate thickness of Si thin films were measured by scanning electron microscopy (SEM, S-3000 N, HITACHI, Japan). The phase structure of was analyzed by X-ray diffraction (XRD, Riguka-D/max 2200, Japan) and high-resolution transmission electron microscopy (HRTEM, JEM-2100F, JEOL, Japan). To evaluate the electrochemical properties of the Si thin film anode, 2025-type half-cells containing Si thin film deposited on Cu foil, separator, electrolyte and lithium foil as counter electrode were assembled in a glove box filled with pure Ar. The electrolyte was 1 M $LiPF_6$/EC:DMC (1:1 in volume) with 1 wt% VC additive. Cyclic voltammetry measurements were performed using an electrochemical workstation (CHI660B, Shanghai Chenhua Instrument Co.) at a scan rate of 0.05 mV s^{-1} in the potential range 0–1.5 V. Charge/discharge tests were carried out using a Land battery test system with the cutoff potentials being 0 V versus Li/Li^+ for discharge and 1.5 V versus Li/Li^+ for charge.

3 Results and discussion

The morphology and thickness of Si thin films were examined by SEM. Figure 1a shows the SEM image of Si thin film deposited on Cu foil. The film has a rough surface, which depends on the surface morphology of the Cu foil substrate. The cross-sectional SEM image of Si thin film deposited on a Si wafer is presented in Fig. 1b. The thickness of the dense Si thin film deposited for 20 min is approximately 275 nm corresponding to a growth rate of 14 nm min^{-1}.

Figure 2 shows the XRD pattern of Si thin film deposited on Cu foil. All the diffraction peaks are attributed to the Cu foil, and no peak of Si appears, especially the typical peak for crystal Si at 28°. This indicates that the Si thin film is amorphous. HRTEM is a more effective method to detect the microstructure of Si thin film. Figure 3 shows the cross-sectional TEM image of Si thin film deposited on a Si wafer. There is no lattice line. The dispersed and very ambiguous selected area electron diffraction (SAED) pattern in the inset of Fig. 3 proves that the Si thin film is completely amorphous. It is reported that the amorphous structure of Si anode material is beneficial to the electrochemical performance because amorphous material shows homogeneous volume expansion/contraction during Li^+ insertion/extraction and has many Li^+ diffusion paths [12].

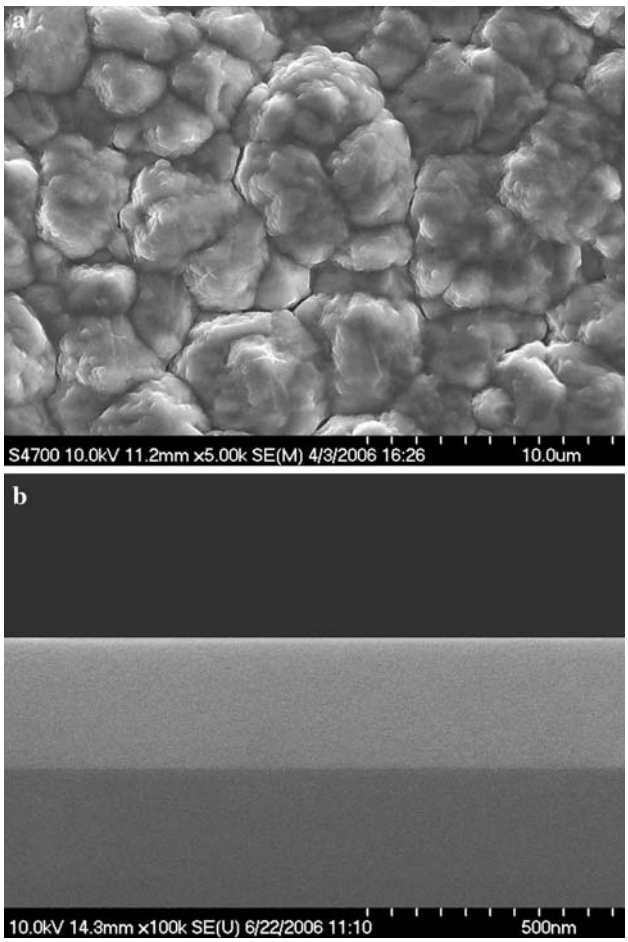

Fig. 1 **a** SEM image of Si thin film deposited on Cu foil. **b** Cross-sectional SEM image of Si thin film deposited on Si wafer

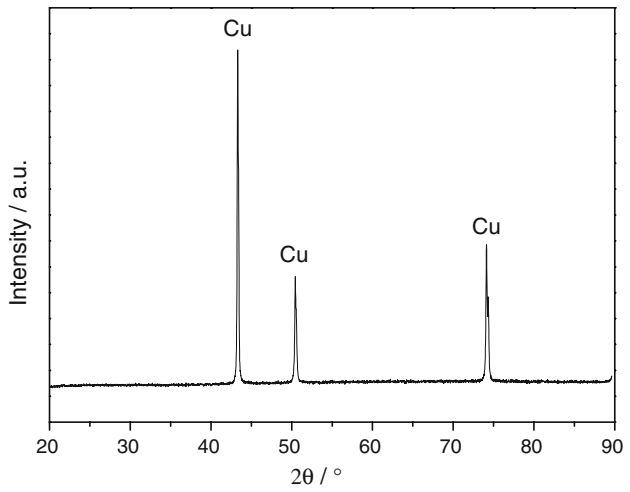

Fig. 2 XRD pattern of Si thin film deposited on Cu foil

The Li^+ insertion/extraction reactions of Si thin film were studied by cyclic voltammetry. Three cyclic voltammetric curves of the Si thin film are shown in Fig. 4. In the first scanning cycle, there is a cathodic peak at 0.50 V, which disappears from the second cycle. This cathodic peak is attributed to the formation of a solid electrolyte interphase (SEI) layer due to decomposition of electrolyte on the film surface [7]. Two cathodic peaks at 0.18 and 0.05 V, as well as two anodic peaks at 0.49 and 0.32 V, are observed on all three cyclic voltammograms; these are ascribed to the electrochemical reactions of Li^+ insertion and extraction in the Si thin film. The slight difference in the intensity and the potential for each peak can be attributed to the kinetic effect involved in the cyclic voltammetry measurement.

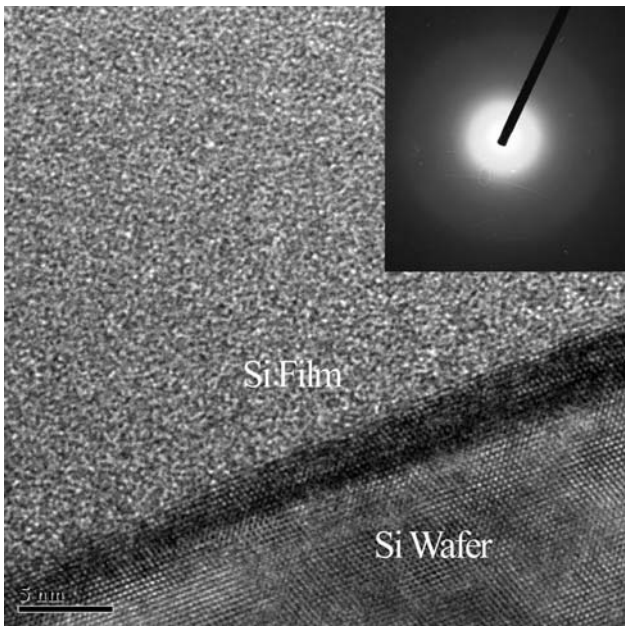

Fig. 3 Cross-sectional HRTEM image of Si film deposited on Si wafer

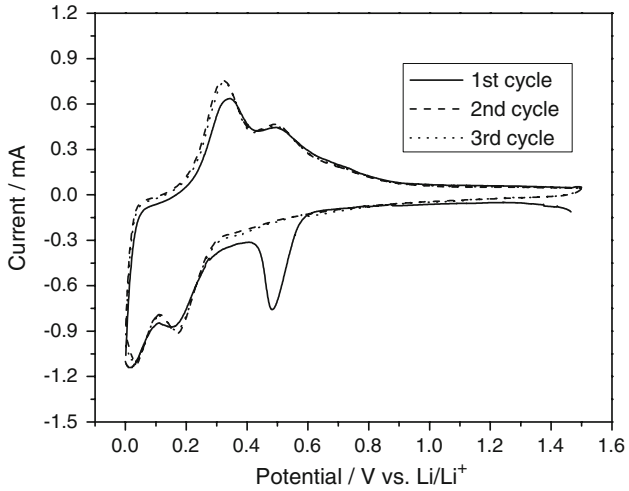

Fig. 4 Cyclic voltammograms of Si thin film at a scan rate of 0.05 mV s^{-1} in the potential range 0–1.5 V

To accurately examine the capacity and voltage plateau of the Si thin film, a small current discharge/charge test was carried out at the rate of 0.025 C. Figure 5 shows the first and second discharge/charge curves of the Si thin film between 0 and 1.5 V versus Li/Li^+. The first discharge capacity and initial coulombic efficiency of the Si thin film are 3,598 mAh g^{-1} and 87.1%, respectively. The first reversible capacity of the Si thin film is 3,134 mAh g^{-1}, which is much higher than that of a graphite anode ($\sim$320 mAh g^{-1}). The irreversible capacity is attributed to the formation of a SEI layer in the first cycle. In evidence, a SEI-formation voltage plateau is observed near 0.4 V, which disappears in the second cycle. This observation is also in good agreement with CV results.

The cycling performance of the Si thin film at 0.5 C rate was examined and the result is shown in Fig. 6. The first

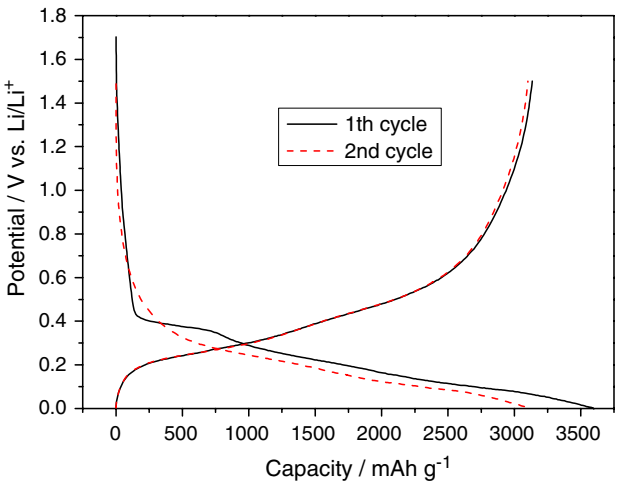

Fig. 5 Discharge/charge curves of Si thin film at the rate of 0.025 C

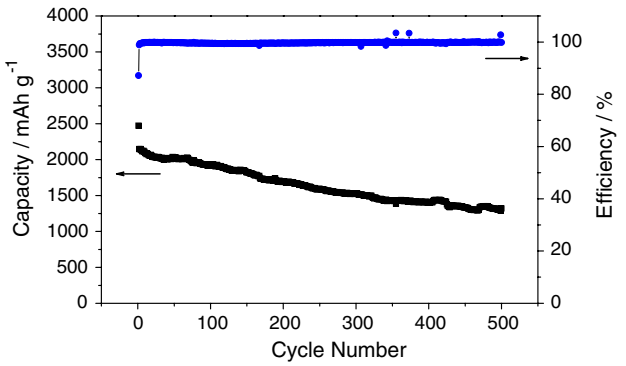

Fig. 6 Cycling performance and coulombic efficiency profiles of Si thin film at 0.5 C rate

reversible capacity of Si thin film at 0.5 C rate is 2,148 mAh g^{-1}. The lower capacity of the Si thin film cycled at a higher rate of 0.5 C compared to 0.025 C rate may be attributed to the kinetic limitation of the alloying of lithium with Si at room temperature. The reversible capacity of the Si thin film is 61.3% of the first reversible capacity even after 500 cycles. Furthermore, the coulombic efficiency of the Si thin film which is 87.2% in the initial cycle at 0.5 C rate increases to above 99% at the second cycle, and maintains a stable value in the subsequent cycles indicating that the film is highly reversible. To find out the mechanism responsible for the long cycling life, the morphology of the Si thin film was observed after cycling. Figure 7 shows the SEM image after cycling 500 times. A series of cracks can be seen on the film surface and some 10–20 μm diameter islands of Si active materials which are caused by mechanical crumbling due to the large volume expansion/contraction in the Li^+ insertion/extraction process are formed. This morphology change is quite different from that of 200 nm Si thin film deposited on smooth Cu foil, which mostly peeled off the substrate after 20 cycles [13]. However, the microstructure closely resembles that of Sn–Co alloy film electrodeposited on rough Cu foil after cycling [18]. It is believed that the rough surface of Cu foil substrate is beneficial for Si thin film to form an island structure. The Si islands adhere strongly to the Cu foil substrate and provide electrical connection. On the other hand, the island structure reduces the stress and strain of Si thin film arising from volume expansion/contraction during cycling. Therefore, the island structure of Si thin film is a possible reason for the long cycling life in this experiment. This indicates that the cycling performance of Si thin film can be further improved by increasing the interface adhesion strength between the Si thin film and Cu foil.

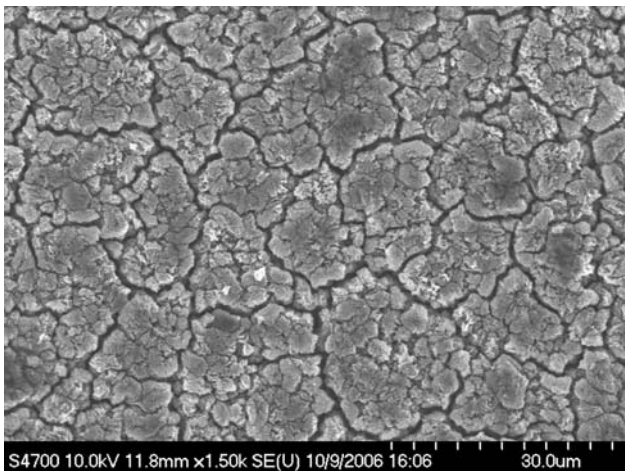

Fig. 7 SEM image of Si thin film cycled 500 times

It is believed that the interface adhesion strength between the Si thin film and Cu foil can be increased by annealing. The Si thin film was annealed at 300 °C for 2 h under inert atmosphere. Figure 8 shows the cycling performance profile of Si thin film after annealing. The capacity retention increased from 61.3% before annealing to 78.5% after annealing for 500 cycles. From the XRD pattern of the annealed Si thin film (inset of Fig. 8), it can be seen that annealing did not change the amorphous structure. Therefore, the main reason for the improvement in cyclability is that annealing enhances the adhesion strength of Si film to the Cu foil substrate because of the interdiffusion of Si and Cu at the film interface. On the other hand, the as-deposited Si thin film is physically bent in a convex form by the residual compressive stress. Annealing eliminates the residual stress to some extent, which is also helpful to the improvement of the cycling performance.

Cyclic voltammetry is often used to study solid-state diffusion of Li^+ in electrode materials [19, 20]. Here, the diffusion coefficient of Li^+ in the Si thin film was measured by cyclic voltammetry. Figure 9 shows cyclic voltammetric curves of Si thin film measured at potential

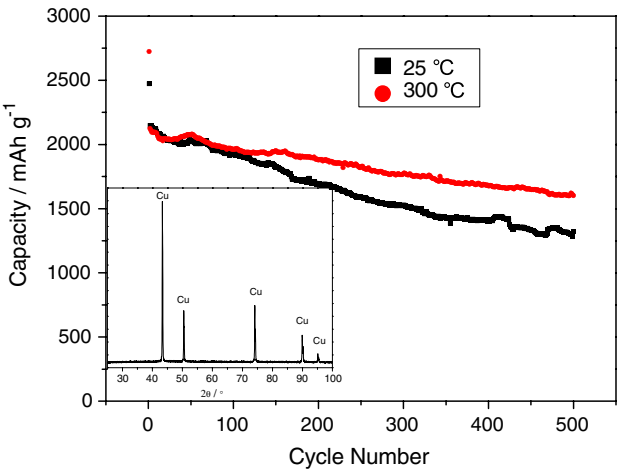

Fig. 8 Comparison of cycling performance of Si thin films before and after annealing

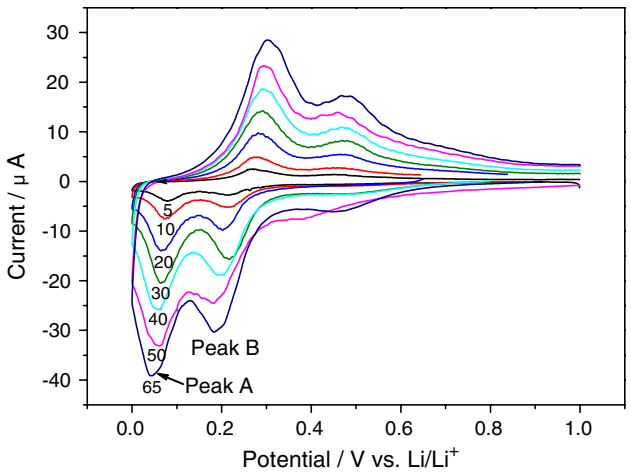

Fig. 9 Cyclic voltammograms for Si thin film at different potential scan rates v μVs^{-1}

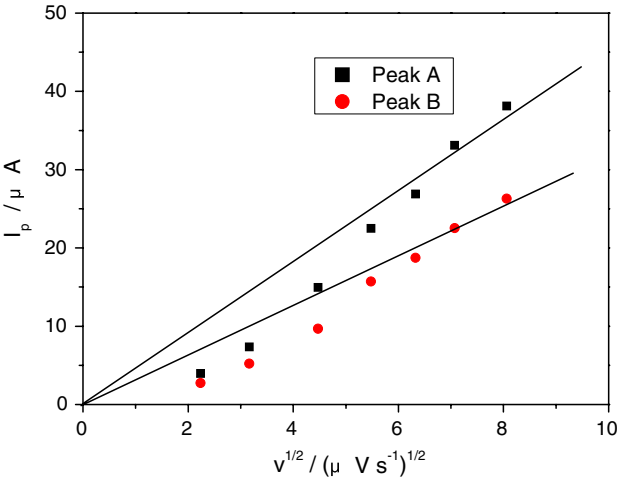

Fig. 10 Dependence of peak currents (I_p) on square root of potential scan rate ($v^{1/2}$) for the two cathodic peaks A and B

scan rates from 5 to 65 μVs^{-1}. Peak currents of both cathodic and anodic peaks increase with increasing potential scan rate. From low scan rate to high scan rate, the rate-determining steps of the electrochemical reaction may change from surface reaction to semi-infinite solid-state diffusion of Li^+. One way to distinguish these different cases is the dependence of the peak current (I_p) on the potential scan rate (v). In the case of surface reaction, the peak current is proportional to scan rate. For the semi-infinite diffusion, the peak current is proportional to the square root of scan rate ($v^{1/2}$), which is expressed by the classical Sevcik equation [19]:

$$I_p = 2.69 \times 10^5 n^{3/2} A D_0^{1/2} v^{1/2} C_0$$

where n is the number of electrons per species reaction (1 for $Li^{+)}$, A is the apparent surface area of the electrode, D_0 is diffusion coefficient of Li^+ in the electrode and C_0 is bulk concentration of Li^+. The dependence of peak current on the square root of the potential scan rate for two cathodic peaks at different scan rates is presented in Fig. 10. I_p is proportional to $v^{1/2}$ when v is above 30 $\mu V\ s^{-1}$. From the slope of I_p versus $v^{1/2}$, we can calculate the apparent diffusion coefficient of Li^+ in the Si thin film assuming semi-infinite diffusion. The calculated diffusion coefficients (D_0) are 1.47×10^{-9} $cm^2 s^{-1}$ and 2.16×10^{-9} $cm^2 s^{-1}$ for peaks A and B, respectively. The Li^+ diffusion coefficient of the Si thin film is larger than that of vacuum-deposited Si film ranging from 10^{-13} to 10^{-10} $cm^2\ s^{-1}$ measured by potential-step chronoamperometry [21].

4 Conclusions

Amorphous Si thin films deposited by magnetron sputtering exhibit high reversible capacity of 3,134 mAh g^{-1} at 0.025 C rate and long cycling life. The capacity retention was 61.3% for 500 cycles at the 0.5 C rate. The surface morphology investigation of the as-deposited and post-cycled Si thin films revealed that the Si thin film formed an island structure after cycling. The Si islands adhere strongly to the Cu foil and reduce the stress and strain arising from volume expansion/contraction during cycling; this results in good cycling performance. Moreover, the capacity retention of Si thin film was further improved to 78.5% for 500 cycles by annealing. This enhanced the interface adhesion strength between Si film and Cu foil. The Li^+ diffusion coefficients of the Si thin film measured by cyclic voltammetry are 1.47×10^{-9} $cm^2\ s^{-1}$ and $2.16 \times 10^{-9} cm^2\ s^{-1}$ for peaks A and B.

References

1. Li H, Huang X, Chen L et al (1999) Electrochem Solid-State Lett 2:547
2. Chen L, Xie X, Wang B et al (2006) Mat Sci Eng B 131:186
3. Chen L, Xie X, Xie J et al (2006) J Appl Electrochem 36:1099
4. Bourderau S, Brousse T, Schleich DM (1999) J Power Sources 81–82:233
5. Jung H, Park M, Yoon Y et al (2003) J Power Sources 115:346
6. Jung H, Park M, Han SH (2003) Solid State Commun 125:387
7. Xia H, Tang S, Lu L (2007) Mater Res Bull 42:1301
8. Ohara S, Suzuki J, Sekine K et al (2004) J Power Sources 136:303
9. Takamura T, Ohara S, Uehara M et al (2004) J Power Sources 129:96
10. Ohara S, Suzuki J, Sekine K et al (2003) J Power Sources 119–121:591
11. Yoshimura K, Suzuki J, Sekine K et al (2005) J Power Sources 146:445
12. Lee K, Jung J, Lee S et al (2004) J Power Sources 129:270
13. Moon T, Kim C, Park B (2006) J Power Sources 155:391
14. Maranchi JP, Hepp F, Kumta PN (2003) Electrochem Solid-State Lett 6:A198

15. Hatchard TD, Dahn JR (2004) J Electrochem Soc 151:A838
16. Beaulieu LY, Hatchard TD, Bonakdarpour A et al (2003) J Electrochem Soc 150:A1457
17. Lee S, Lee J, Chung S et al (2001) J Power Sources 97–98:191
18. Tamura N, Fujimoto M, Kamino M et al (2004) Electrochim Acta 49:1949
19. Levi MD, Aurbach D (1997) J Electroanal Chem 421:79
20. Wu M, Chiang PJ (2006) Electrochem Commun 8:383
21. Yoshimura K, Suzuki J, Sekine K et al (2005) J Power Sources 14:445